New Full-Vectorial Numerically Efficient Propagation Algorithm Based on the Finite Element Method

S. S. A. Obayya, B. M. A. Rahman, *Senior Member, IEEE,* and H. A. El-Mikati

***Abstract*—A new full-vectorial beam propagation algorithm based on the versatile finite element method, in order to accurately characterize three-dimensional (3-D) optical guided-wave devices, is presented. The computationally efficient formulation is based on the two transverse components of the magnetic field without destroying the sparsity of the matrix equation. The robust perfectly matched layer (PML) boundary condition is incorporated into the formulation so as to effectively absorb the unwanted radiation out of the computational domain. The efficiency and precision of the proposed full-vectorial propagation approach is demonstrated through the analysis of single optical waveguide, directional couplers, and electrooptic modulator.**

***Index Terms*—Beam propagation method (BPM), directional couplers (DC's), finite element method (FEM), optical waveguides, photonic devices.**

I. Introduction

MODAL solutions are very useful for the characterization of uniform optical waveguides, and many semi-analytical and numerical modal solution approaches have been reported. It has been shown that the vector finite element method (VFEM) is an accurate and powerful method to find the modal solutions for a wide range of optical waveguides [1]. Many photonic devices may consist of a few butt-coupled uniform guided-wave sections, such as the directional coupler or multimode-interference (MMI)-based devices. By accurately calculating the even and odd supermode propagation constants, the VFEM is capable of calculating the coupling length, however, the VFEM cannot directly estimate the power coupling efficiency between coupled guides. Earlier, it has been shown that a combination of the VFEM and the least squares boundary residual (LSBR) method can accurately characterize directional couplers [2], or MMI-based devices [3], i.e., devices with a finite number of longitudinal discontinuities. However, to design three-dimensional (3-D) photonic devices with arbitrary axial variations, a more versatile numerical approach, like the beam propagation method (BPM), is mandatory. Feit and Fleck [4] introduced the fast-Fourier transform (FFT)-based BPM to simulate axially nonuniform structures, however, their approach is only suitable for weakly guiding waveguides. Since then, many scalar, semi-vectorial and full-vectorial BPM approaches based on the popular finite difference method (FDBPM) have been reported [5]–[7]. Due to the inefficient discretization associated with finite differences, the FDBPM needs large computational resources especially in simulating nonuniform optical waveguides. Due to its numerical efficiency and versatility, some BPM algorithms have been formulated based on the finite element method [8], [9]. However, most of these finite element-based BPM algorithms are solving the less accurate, albeit simpler, scalar wave equation which cannot accurately model the wave propagation in three-dimensional optical waveguides with hybrid fields. A full vectorial approach is particularly necessary to calculate the polarization conversion in the optical guided-wave devices or systems. Recently, a vectorial BPM algorithm based on the finite element method has been reported [10], however, the algorithm is solving for the three magnetic field components and is not incorporating a robust boundary condition to effectively absorb the outgoing radiations.

In this paper, a new full-vectorial BPM algorithm based on the numerically efficient finite element method (VFEBPM) is presented. This algorithm considers only two transverse magnetic field components, hence it is more numerically efficient than the vectorial propagation algorithm which considers all the three magnetic field components [10]. Recently, a robust perfectly matched layer (PML) boundary condition [11] has been introduced to the finite element based BPM formulations, but either considering a simple scalar formulation [12] or an $\mathbf{E}$-field formulation [13], which considers all the three field components. In the present work, the PML boundary condition is incorporated to the newly developed full-vectorial FE-based BPM approach. As it will be shown later on, the sparsity of the global matrices is retained as no matrix inversion is needed, hence, a numerically efficient sparse matrix solver is used which is the main advantage of the present formulation. In Section II, the main theory of the new full-vectorial BPM algorithm will be presented. To test the accuracy of the proposed BPM, it will be applied to some optical waveguide devices and the results, presented in Section III, will be compared with those obtained from other rigorous vectorial methods.

II. Theory

From the Maxwell's two curl equations, the vector wave equation based on the magnetic field vector, $\mathbf{H}$, can be derived:

$$\nabla \times (n^{-2} \nabla \times \mathbf{H}) - k^2 \mathbf{H} = 0 \tag{1}$$

Manuscript received April 16, 1999; revised October 29, 1999.

S. S. A. Obayya and H. A. El-Mikati are with the Department of Electrical Communications, Mansoura University, Mansoura, Egypt.

B. M. A. Rahman is with the Department of Electrical, Electronic, and Information Engineering, City University, Northampton Square, London EC1V 0HB, U.K. (e-mail: B.M.A.Rahman@City.ac.uk).

Publisher Item Identifier S 0733-8724(00)02191-5.

where k and n are the free space wavenumber and the refractive index, respectively, and the del operator, ∇, used in (1) is defined as

$$\nabla = i_x\alpha_x\frac{\partial}{\partial x} + i_y\alpha_y\frac{\partial}{\partial y} + i_z\alpha_z\frac{\partial}{\partial z} = \nabla_t + i_z\alpha_z\frac{\partial}{\partial z} \quad (2)$$

with i_x, i_y, and i_z are the unit vectors associated with x, y, and z directions, respectively, and α_x, α_y, and α_z are parameters associated with the PML boundary condition. Since the waves are assumed to propagate in z direction, the parameter α_z will be set to unity, while the other PML parameters have to be determined such that the wave impedance of the PML layer placed around the computational domain is exactly the same as that of the adjacent medium inside the computational domain. Hence, the PML medium will perfectly matches the computational domain medium which will allow the unwanted radiations to leave the computational domain freely without any reflection. This necessary condition can be derived as [11]

$$\alpha_{x,y} = \frac{1}{1 - j\frac{\sigma_e}{\omega\varepsilon_0 n^2}} = \frac{1}{1 - j\frac{\sigma_m}{\omega\mu_0}} \quad (3)$$

where ω, ε_0, and μ_0 are the angular frequency, the free space permittivity and permeability, respectively, while σ_e and σ_m are the electric and magnetic conductivity profiles of the PML, respectively. If a parabolic electric conductivity profile is assumed, then [11]

$$\alpha_{x,y} = 1 - j\frac{3\lambda\rho^2}{4\pi n d^3}\ln\left(\frac{1}{R}\right) \quad (4)$$

where λ is the wavelength, d is the width of PML (kept constant in all directions), ρ is the distance inside the PML measured from the PML-computational domain interface, and R is the allowable theoretical value of the reflection coefficient at the PML-computational domain interface, which is set to a very small value during the simulations. The parameters α_x and α_y are set in different regions as follows. Inside the orthodox computational domain, both α_x and α_y are set to unity, while for PML regions faced normally with x direction, α_x is set as indicated in (4) while α_y is set to unity, and the situation is reversed for PML regions normally faced with y direction. For corners, both α_x and α_y are set as indicated in (4). With these PML arrangements in different regions, any radiation wave will freely leave the computational domain whatever the angle it hits the PML-computational domain boundaries, and this kind of PML boundary condition has been used with the scalar one-dimensional FDBPM [14] to show its effectiveness over the transparent boundary condition [15]. However, the incorporation of the PML boundary condition into the full-vectorial BPM formulation is, to best of our knowledge, presented here for the first time.

Using the zero divergence condition of the magnetic field, $\nabla \cdot \mathbf{H} = 0$, and decomposing the transverse magnetic field vector, $\mathbf{H}_t$, into a slowly z-varying vector envelope, ψ_t, and a fast oscillating-phase, then, (1) for the transverse slowly varying envelope, ψ_t, takes the form

$$n^{-2}\frac{\partial^2\Psi_t}{\partial z^2} - 2jn_0kn^{-2}\frac{\partial\Psi_t}{\partial z} + n^{-2}\nabla_t(\nabla_t\cdot\Psi_t) - \nabla_t\{n^{-2}(\nabla_t\times\Psi_t)\cdot i_z\}\times i_z + k^2\left(1 - n^{-2}n_0^2\right)\Psi_t = 0 \quad (5)$$

where n_0 is the reference index of refraction. If the waveguide cross section is divided into a number of first-order triangular elements, the application of Galerkin's procedure to (5) results in

$$\begin{aligned}&\int_A N_i n^{-2}\frac{\partial^2\Psi_t}{\partial z^2}\,dA - 2jn_0k\int_A N_i n^{-2}\frac{\partial\Psi_t}{\partial z}\,dA \\ &\quad - \int_A \nabla_t N_i n^{-2}(\nabla_t\cdot\Psi_t)\,dA + \oint_l n^{-2}N_i(\nabla_t\cdot\Psi_t)n_l\,dl \\ &\quad + \int_A (\nabla_t N_i)\times i_z\{n^{-2}(\nabla_t\times\Psi_t)\cdot i_z\}\,dA \\ &\quad - \oint_l N_i n_l\times i_z\{n^{-2}(\nabla_t\times\Psi_t)\cdot i_z\}\,dl \\ &\quad + k^2\int_A N_i\left(1 - n^{-2}n_0^2\right)\Psi_t\,dA = 0\end{aligned} \quad (6)$$

where N_i is the weight function which is assumed the same as the shape function at the ith node ($i = 1,2,3$), A is the element area, l is the element boundary, and n_l is the unit vector in the direction of the outward normal to the element boundary. The evaluation of the line integrations involved in (6) is mandatory in order to account for the interface boundary conditions between elements with different materials. The second line integral appearing in (6) is proportional to the longitudinal electric field components, E_z, which is continuous everywhere, and hence, its contribution along all the inter-element boundaries will cancel, even when the adjacent elements have different refractive indices. On the other hand, the first line integral in (6) has to be calculated, *but only* along the interfaces between two elements with different refractive indices, as it accounts for the discontinuity of the transverse magnetic field derivatives. It can be shown that only the first line integral of (6) is responsible for both polarization dependence and coupling. Hence, working with transverse magnetic field formulation is more advantageous not only because of the more economical use of the computational resources, but also, as it rigorously enforces the interface boundary conditions. Hence, the spurious nonphysical solutions are not permitted to propagate: a problem commonly arises with most of the vector formulations.

Performing the integrations involved in (6) and collecting the contributions from all elements leads to the following nonparaxial vector wave equation:

$$[\mathbf{M}]\frac{d^2\{\mathbf{h_t}\}}{dz^2} - 2jn_0k[\mathbf{M}]\frac{d\{\mathbf{h_t}\}}{dz} + \left([\mathbf{K}] - n_0^2k^2[\mathbf{M}]\right)\{\mathbf{h_t}\} = \{\mathbf{0}\} \quad (7)$$

where $\{\mathbf{h_t}\}$ represents a column vector containing all the nodal values of the slowly varying transverse magnetic field compo-

nents, $\{\mathbf{0}\}$ is a null column vector, and $[\mathbf{M}]$ and $[\mathbf{K}]$ are the global element matrices assembling the contributions from all elements, which can be expressed as

$$[\mathbf{M}] = \sum_e \begin{bmatrix} [M_{xx}] & [0] \\ [0] & [M_{yy}] \end{bmatrix} \tag{8}$$

$$[\mathbf{K}] = \sum_e \begin{bmatrix} [K_{xx}] & [K_{xy}] \\ [K_{yx}] & [K_{yy}] \end{bmatrix} \tag{9}$$

with

$$[M_{xx}] = [M_{yy}] = \left[n^{-2} \int_A N_i N_j \, dA \right] \tag{10}$$

$$[K_{xx}] = \left[\int_A \left(k^2 N_i N_j - n^{-2} \alpha_x^2 N_{ix} N_{jx} - n^{-2} \alpha_y^2 N_{iy} N_{jy} \right) dA + \oint_l n^{-2} \alpha_x^2 N_i N_{jx} l_x \, dl \right] \tag{11}$$

$$[K_{yy}] = \left[\int_A \left(k^2 N_i N_j - n^{-2} \alpha_x^2 N_{ix} N_{jy} - n^{-2} \alpha_y^2 N_{iy} N_{jy} \right) dA + \oint_l n^{-2} \alpha_y^2 N_i N_{jy} l_y \, dl \right] \tag{12}$$

$$[K_{xy}] = \left[\int_A (n^{-2} \alpha_x \alpha_y N_{iy} N_{jx} - n^{-2} \alpha_x \alpha_y N_{ix} N_{iy}) \, dA + \oint_l n^{-2} \alpha_x \alpha_y N_i N_{jy} l_x \, dl \right] \tag{13}$$

$$[K_{yx}] = \left[\int_A (-n^{-2} \alpha_x \alpha_y N_{iy} N_{jx} + n^{-2} \alpha_x \alpha_y N_{ix} N_{jy}) \, dA + \oint_l n^{-2} \alpha_x \alpha_y N_i N_{jx} l_y \, dl \right] \tag{14}$$

where $\sum_e$ stands for summation of contributions from all elements, $i, j = 1, 2, 3$, l_x and l_y are the direction cosines between the outward normal unit vector, n_l, and the x and y directions, respectively, and $[0]$ is a 3×3 null matrix. In solving (7), the Padè approximation [16] has been utilized to derive the first-order wide-angle wave equation as

$$-2jn_0k[\mathbf{L}] \frac{d\{\mathbf{h_t}\}}{dz} + \left([\mathbf{K}] - n_0^2 k^2 [\mathbf{M}] \right) \{\mathbf{h_t}\} = \{\mathbf{0}\} \tag{15}$$

with

$$[\mathbf{L}] = [\mathbf{M}] + \frac{1}{4n_0^2 k^2} \left([\mathbf{K}] - n_0^2 k^2 [\mathbf{M}] \right) \tag{16}$$

Dividing the z-direction into a number of elements each with a width of Δz, and applying Galerkin's method to the wide-angle wave equation results in

$$[\mathbf{A}]_m \{\mathbf{h_t}\}_{m+1} = [\mathbf{B}]_m \{\mathbf{h_t}\}_m \tag{17}$$

with

$$[\mathbf{A}]_m = -2jn_0k[\mathbf{L}]_m + \theta \Delta z \left\{ [\mathbf{K}]_m - n_0^2 k^2 [\mathbf{M}]_m \right\} \tag{18}$$

$$[\mathbf{B}]_m = -2jn_0k[\mathbf{L}]_m + (\theta - 1) \Delta z \left\{ [\mathbf{K}]_m - n_0^2 k^2 [\mathbf{M}]_m \right\} \tag{19}$$

where Δz is the propagation step size, θ is the propagation scheme parameter, and the subscripts m and $m+1$ stand for quantities related to the mth and $m+1$th propagation steps, respectively. The stability range for the propagation algorithm is $\theta \geq 0.5$. During the numerical simulations $\theta = 0.5$, the Crank–Nicolson algorithm, will be adopted as it is stable and also the least dissipating of the propagating power.

III. Numerical Examples

To assess the numerical precision of the proposed VFEBPM, it is first applied to a single rectangular guide shown in the inset of Fig. 1. The refractive index of the core, n_g, is 3.26 while that of the substrate, n_s, is 3.20 and the simulation is carried out at a wavelength of 1.3 μm. In all simulations, the width of the PML layer is taken as 1.0 μm, the theoretical reflection coefficient, R, as 10^{-100}, and the reference refractive index, n_0, as the mean value of the core and substrate indexes. In this example, the waveguide cross section is represented by 7200 first-order triangular elements. The waveguide is launched with the fundamental transverse electric (TE) or transverse magnetic (TM) modal field profiles obtained from the VFEM [1]. Fig. 1 shows the effect of the propagation step size, Δz, on the level of numerical dissipation for both TE and TM modes. Each of the simulation points shown in Fig. 1 takes around 10 min on SUN 4/85 Workstation. It is suspected that some stable numerical algorithm may not conserve the propagating beam power. However, it can be noted from Fig. 1 that for the range of $\Delta z < 2.0$ μm, the nonphysical power loss is less than 0.00002 dB/mm for both the polarizations. With this extremely low nonphysical power loss, the proposed VFEBPM can be regarded as a stable and power conserving technique as well. Next, the capability of the proposed VFEBPM as a "mode solver" is investigated. Launching an arbitrary initial field into the considered rectangular waveguide, and letting it to propagate along the imaginary axis, the fundamental TE or TM mode will be evolved [17]. To test the accuracy of the solution, a simple rectangular spatial pulse with sharp step rise is launched into the waveguide. For TE excitation, the field profile of its dominant H_y component at $z = 50$ µm is shown in Fig. 2. This field profile resembles the fundamental TE mode after propagating a relatively short distance of 50 μm. The variation of the effective indices, $n_e = \beta/k$, where β is the mode propagation constant, for both TE and TM modes with the imaginary propagation distance are also calculated. These effective index values settle to 3.241 25, and 3.24121 for TE and TM modes, respectively, after propagating a distance of around 40 μm along the imaginary axis. The same fundamental TE and TM modes have also been rigorously solved by using the VFEM [1] with 12 800 first-order triangular elements to discretize the waveguide cross section. The variation of the percentage errors in calculating the TE and TM effective indices using the VFEBPM are shown in Fig. 3. It

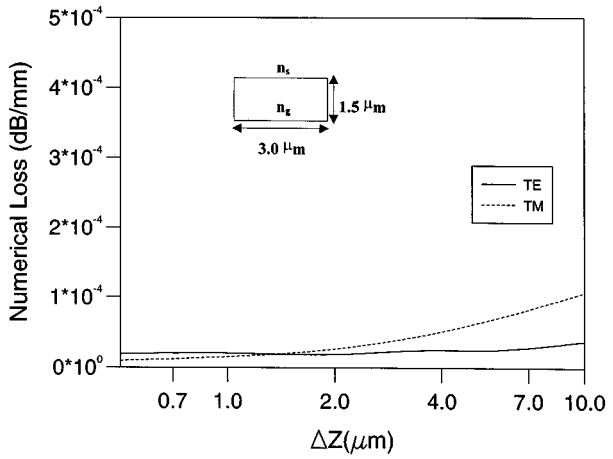

Fig. 1. Effect of the propagation step size on the nonphysical power loss for both TE and TM waves. The inset is a schematic diagram of the rectangular guide under consideration.

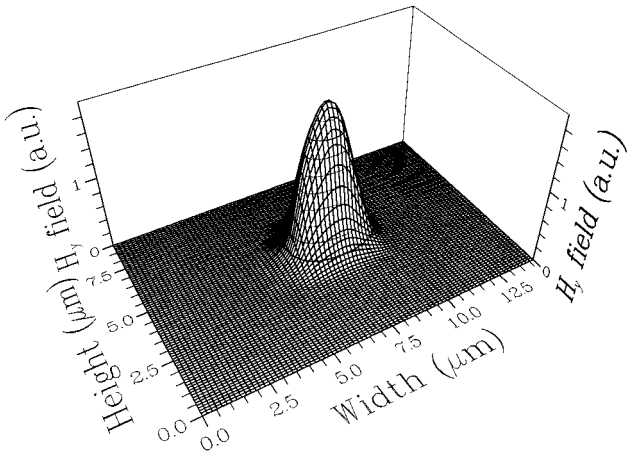

Fig. 2. Contour plot of the H_y-field profile for the fundamental quasi-TE mode at $z = 50$ μm.

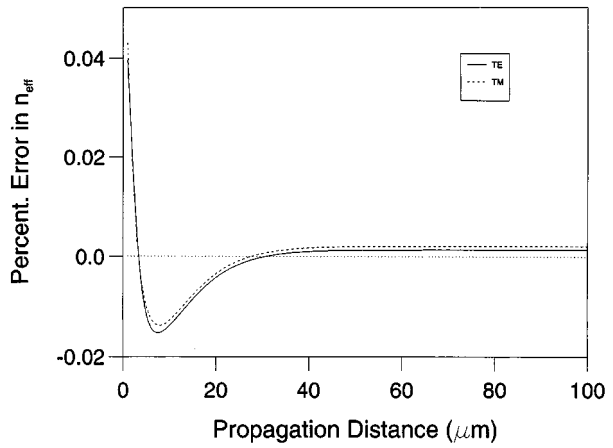

Fig. 3. Variation of the errors in the n_e calculation of the fundamental TE and TM modes with the longitudinal imaginary distance.

may be observed from this figure that the percentage errors in calculating the effective indexes using the VFEBPM were only 0.0012% and 0.0018% for TE and TM modes, respectively. This proves the accuracy of the proposed VFEBPM approach.

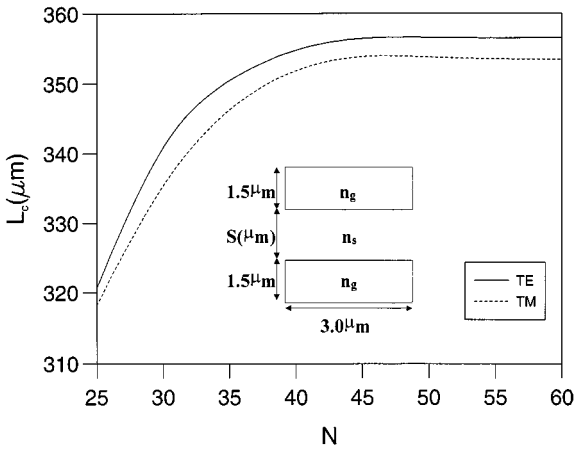

Fig. 4. Effect of the transverse mesh divisions on the coupling lengths of TE and TM waves. The inset is a schematic diagram of the directional coupler under consideration.

Next, a simple rectangular directional coupler consisting of two-vertically coupled rectangular guides, shown in the inset of Fig. 4, is simulated at a wavelength of 1.3 μm. Initially, the core index, n_g, and the substrate index, n_s, are assumed as 3.26 and 3.20, respectively, and the waveguide separation, S, is taken as 0.8 μm. Launching one of the guides with its isolated TE or TM fundamental modal field profile, the coupling length can be defined as the minimum distance at which a maximum power transfer between guides occurs. The effect of transverse mesh divisions on the coupling length for both TE and TM polarized waves is shown in Fig. 4, where N is the number of divisions in either x or y direction. In this case, Δz is taken as 0.5 μm. It can be noted from Fig. 4 that for $N > 45$, the coupling lengths settle to 357 μm and 353 μm for TE and TM polarized waves, respectively. For $N = 60$, in both transverse directions, the effect of Δz on the coupling length for both TE and TM polarized waves is shown in Fig. 5, where it can be observed that the coupling lengths for TE and TM polarized waves are virtually constant for $\Delta z < 1.0$ μm. In order to assess the accuracy of the VFEBPM in calculating the coupling length, the same directional coupler structure has also been analyzed using the VFEM [1] with 12 800 first-order triangular elements. Through the calculation of the propagation constants of the even and odd supermodes using the VFEM, the coupling length, L_c, for either polarization can be calculated as

$$\mathbf{L_c} = \frac{\pi}{\beta^e - \beta^o} \tag{20}$$

where β^e and β^o are the propagation constants of the even and odd supermodes, respectively. For this coupler, the coupling lengths obtained by using the VFEM were 356.2 and 354.2 μm for TE and TM polarizations, respectively. It can be noted that the percentage difference between the coupling length results obtained using the VFEBPM and the VFEM are 0.22% and 0.34% for TE and TM polarizations, respectively, which shows the high numerical accuracy of the newly developed VFEBPM, in calculating the coupling length for both TE and TM polarizations. Next, the effect of varying both the waveguide separation, S, and the core index, n_g, on the TE and TM coupling length

is shown in Fig. 6. In all cases, it may be noted that the coupling lengths for TE and TM increase exponentially (linear for semi-log scale) with the increase of S. For lower core indices, cases "a", $n_g = 3.26$, and "b", $n_g = 3.3$, the polarization effect on the coupling length is negligible. However, for case "c", $n_g = 3.4$, the coupling length for TM is relatively higher than its TE counterpart. These features related to polarization effect on the coupling length cannot be accurately predicted using a less accurate scalar BPM algorithms. In all cases, the TE and TM coupling lengths have been recalculated using the VFEM with 12 800 first-order triangular elements and the differences between these results and those obtained using the VFEBPM were always less than 0.8%. It can be noted that accuracy of the solutions may be improved by using a finer mesh discretization.

Next, a simple rib directional coupler, shown in the inset of Fig. 7, is simulated using the VFEBPM at a wavelength of 1.55 μm. For this coupler, the substrate index, n_s, is taken as 3.4, and the rib width, W, is kept constant at 3.0 μm, while the guide index, n_g, and the waveguide separation, S, are varied. In the VFEBPM simulations, the structure cross section is divided into 6400 first-order triangular elements, and Δz is taken as 1.0 μm. For two values of the index difference, $\Delta n = n_g - n_s$, the effect of waveguide separation on the TE coupling length is shown in Fig. 7. As shown in this figure, the increase of S and/or Δn leads to the increase of the coupling length. The same simulation points have been also carried out using the VFEM [1] and the coupling lengths obtained using the VFEBPM differ only 1%. Although the VFEM is very accurate in finding the coupling lengths, however, it cannot directly estimate the crosstalk arises due to the incomplete power transfer between guides. On the other hand, the VFEBPM can accurately calculate the power evolution in a system of coupled waveguides. The crosstalk for a directional coupler can be defined as

$$\text{Crosstalk (dB)} = 10\log_{10}\left(\frac{P_a(z=L_c)}{P_b(z=L_c)}\right) \qquad (21)$$

where $P_a(z=L_c)$ and $P_b(z=L_c)$ are the powers belonging to guides "a", and "b", respectively, calculated at a longitudinal position equals to the coupling length. In (21), it has been assumed that guide "a" is initially excited. Crosstalk is an important optical parameter for characterizing directional couplers. For TE excitation, the effect of the device length, L_c, on the crosstalk for two values of the index difference, Δn, is shown in Fig. 8. It can be observed that the crosstalk associated with a directional coupler can be improved by increasing its length. It may be noted that for $\Delta n = 0.04$ and a device length of 1000 μm, the crosstalk level is -18.5 dB, however, increasing Δn to 0.06 and keeping the same device length at 1000 μm, the crosstalk level is improved to -21.5 dB.

Finally, as an example of a nonidentical directional coupler, an electrooptic $LiNbO_3$ channel coupler modulator, shown in the inset of Fig. 9, is simulated at a wavelength of 0.85 μm. Without any applied modulating signal, the refractive index of both $LiNbO_3$ guides, n_g, is taken as 2.3, while that of the cladding, n_s, is 2.29. With appropriate electrode design, for nonzero modulating potential, it is assumed that the index in one guide increases while in the other guide decreases by the same amount, $\Delta n/2$, and the cladding index remains constant.

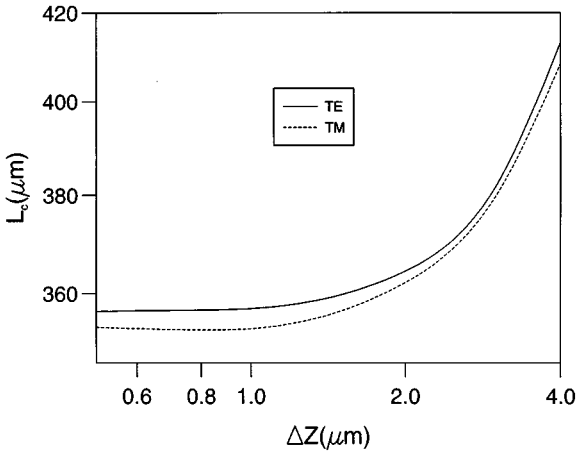

Fig. 5. Effect of the propagation step size (Δz) on the coupling lengths of TE and TM waves.

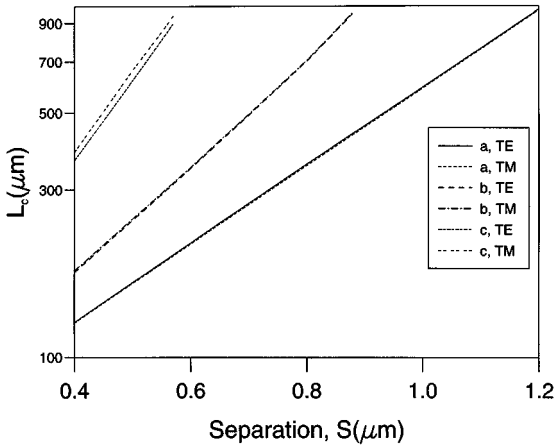

Fig. 6. Variation of TE and TM coupling lengths with the waveguide separation (S) and the index difference (Δn) as a parameter.

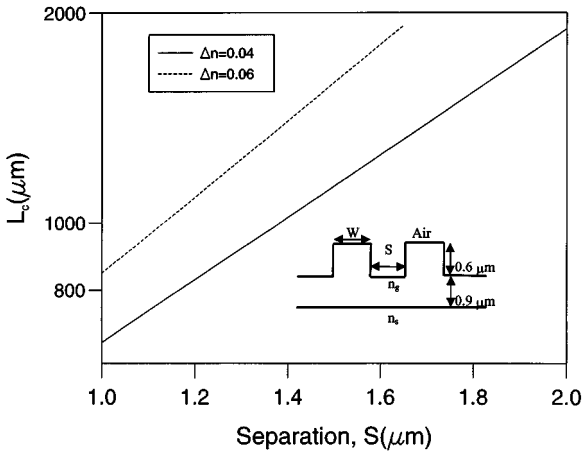

Fig. 7. Variation of TE coupling length with the waveguide separation (S) and the index difference (Δn) as a parameter. The inset is a schematic diagram of the rib directional coupler under consideration.

The effect of electrooptically induced index difference, Δn, on the TE coupling length is shown in Fig. 9, where the results obtained using the VFEBPM and VFEM [2] are in close agreement. Without applied modulating potential, $\Delta n = 0$, the two guide are phase matched giving rise to a peak coupling length,

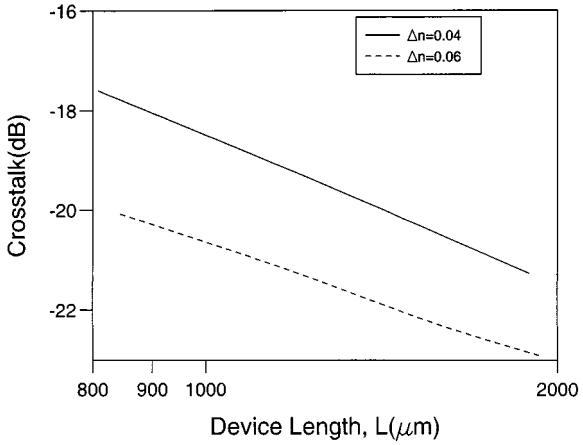

Fig. 8. Variation of the crosstalk with the device length and the index difference as a parameter.

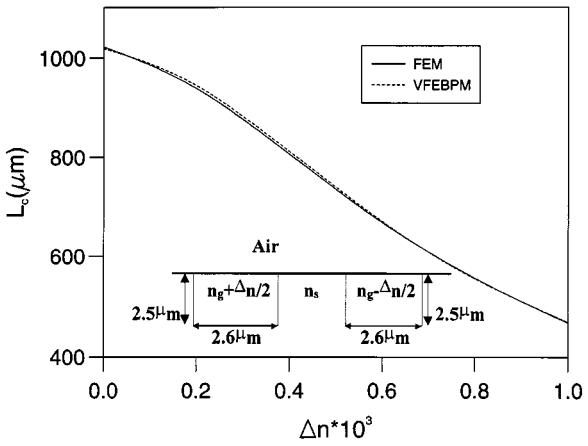

Fig. 9. Effect of the electrooptically induced index difference on the coupling length. The inset is a schematic diagram of the electrooptic $LiNbO_3$ channel coupler modulator under consideration.

1010 μm, which monotonically reduces with the increase of Δn as the two guides keep on losing their synchronousity. When the input power is launched into guide "b", the power evolution in the two guides with the axial direction, z, is shown in Fig. 10 for two values of Δn. For $\Delta n = 0$, full power transfer from guide "b" to guide "a" can be observed at around 1010 μm, while for $\Delta n = 0.00092$, a fraction of the guide "b" power is initially transferred to guide "a" due to their phase mismatch, then, this power is returned again to guide "b" with virtually no overall power is transferred to guide "a". It can be noted that, when $\Delta n = 0.00092$, the coupling length, L_c, is equal to 505.0 μm, half of the value for $\Delta n = 0$. In this case, at $z = L_{\rm co}$, the optical power couples back to guide "b" as shown in Fig. 10. With guide "a" as an output port, the variations of the maximum and output powers, $P_{\max}$ and P_o, with Δn are shown in Fig. 11. The maximum power, $P_{\max}$, is the power transferred to guide "a" at a device length equals to the coupling length at the concerned Δn, while the output power, P_o, denotes the power transferred to guide "a" at a fixed device length equals to the peak coupling length, $L_{\rm co} = 1010$ μm. The power transfer results obtained using the VFEBPM are in excellent agreement with those obtained using the LSBR method [2]. As shown in Fig. 11, the output power is minimum for Δn values at which $L_{\rm co}$ is an even multiple of the coupling length, while for Δn values at which $L_{\rm co}$ is an odd multiple of the coupling length, the output power reaches a maximum value but not reaching the unity peak as the two guides are strongly phase mismatched and hence, the full power transfer is inhibited.

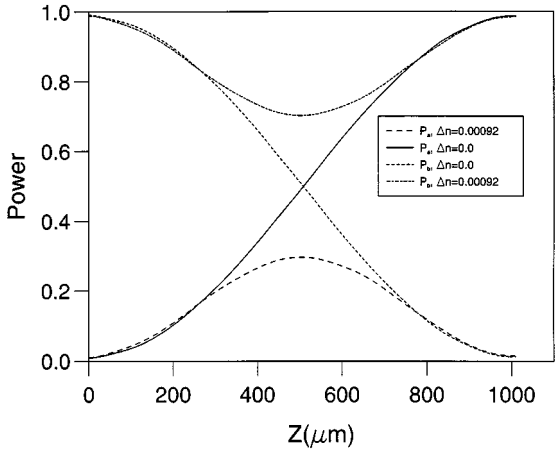

Fig. 10. The evolution of optical power in the two guides along the axial direction.

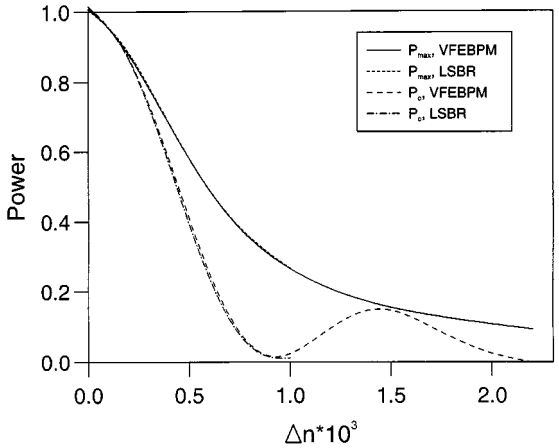

Fig. 11. Variations of the output (P_o) and maximum powers ($P_{\max}$), with the electrooptically induced index difference.

IV. Conclusion

A new full-vectorial propagation algorithm based on the numerically efficient finite element method is presented for the accurate characterization of 3-D optical guided-wave devices. The new vector formulation is based on the transverse magnetic field components allows effectively to account for the interface boundary conditions between different dielectric media. As no matrix inversion is needed in deriving the global matrices, the resulting matrices are sparse which can be solved using any numerically efficient sparse matrix solver. Also, for the first time, the robust PML boundary condition is incorporated into the new full vectorial BPM formulation in order to offer a reflectionless boundary for the radiation waves. Through comparisons with other full vectorial approaches, the numerical accuracy of the proposed full-vectorial FE-based BPM algorithm has been demonstrated through the analyzes of different photonic

devices, including, single rectangular guide, rectangular directional coupler, rib directional coupler, and electrooptic $LiNbO_3$ directional coupler-based modulator. Hence, the proposed full vectorial BPM approach can be used to accurately model and optimize the performance of different 3-D photonic devices including structures with totally arbitrary variation along the axial direction.

REFERENCES

[1] B. M. A. Rahman and J. B. Davies, "Finite-element analysis of optical and microwave waveguide problems," *IEEE Trans. Microwave Theory Tech.*, vol. 32, pp. 20–28, 1984.

[2] T. Wongchareon, B. M. A. Rahman, and K. T. V. Grattan, "Electro-optic directional coupler switches characterization," *J. Lightwave Technol.*, vol. 15, pp. 377–382, Feb. 1997.

[3] M. Rajarajan, B. M. A. Rahman, T. Wongchareon, and K. T. V. Grattan, "Accurate analysis of MMI devices with two-dimensional confinement," *J. Lightwave Technol.*, vol. 14, pp. 2078–2084, Sept. 1996.

[4] M. D. Feit and J. A. Fleck, "Computation of mode properties in optical fiber waveguides by a beam propagation method," *Appl. Opt.*, vol. 19, pp. 1154–1164, 1980.

[5] Y. Chung, N. Dagli, and L. Thylen, "Explicit finite difference vectorial beam propagation method," *Electron. Lett.*, vol. 27, no. 23, pp. 2119–2121, 1991.

[6] J. Van Roey, J. Van der Donk, and P. Lagasse, "Beam-propagation method: Analysis and assessment," *J. Opt. Soc. Amer.*, vol. 71, no. 7, pp. 803–810, 1981.

[7] P. C. Lee and E. Voges, "Three-dimensional semi-vectorial wide-angle beam propagation method," *J. Lightwave Technol.*, vol. 12, pp. 215–225, Feb. 1995.

[8] F. Schmidt, "An adaptive approach to the numerical solution of Fresnel's wave equation," *J. Lightwave Technol.*, vol. 11, pp. 1425–1434, Sept. 1993.

[9] K. Hayata, A. Misawa, and M. Koshiba, "Split-step finite element method applied to nonlinear integrated optics," *J. Opt. Soc. Amer. B*, no. 9, pp. 1772–1784, 1990.

[10] E. Montanari, S. Selleri, L. Vincetti, and M. Zoboli, "Finite-element full-vectorial propagation analysis for three-dimensional z-varying optical waveguides," *J. Lightwave Technol.*, vol. 16, pp. 703–714, Apr. 1998.

[11] J. P. Berenger, "A perfectly matched layer for the absorption of electromagnetic waves," *J. Comput. Phys.*, vol. 114, no. 10, pp. 185–200, 1994.

[12] M. Koshiba, Y. Tsuji, and M. Hikari, "Finite element beam propagation method with perfectly matched layer boundary conditions," *IEEE Trans. Magn.*, vol. 35, pp. 1482–1485, 1999.

[13] F. Fogli, G. Bellanca, and P. Bassi, "TBC and PML conditions for 2D and 3D-BPM: A comparison," *Opt. Quantum Electron.*, vol. 30, pp. 443–456, 1998.

[14] W. P. Huang, C. L. Xu, W. Lui, and K. Yokoyama, "The perfectly matched layer (PML) boundary condition for the beam propagation method," *IEEE Photon Technol. Lett.*, vol. 8, pp. 649–651, May 1996.

[15] G. R. Hadley, "Transparent boundary condition for the beam propagation method," *Opt. Lett.*, vol. 16, no. 5, pp. 621–626, 1991.

[16] G. R. Hadley, "Wide-angle beam propagation using Pade approximation operators," *Opt. Lett.*, vol. 17, no. 10, pp. 1426–1428, 1992.

[17] C. L. Xu, W. P. Huang, and S. K. Chaudhuri, "Efficient and accurate vector mode calculations by beam propagation method," *J. Lightwave Technol.*, vol. 11, pp. 1209–1215, July 1993.

S. S. A. Obayya, photograph and biography not available at the time of publication.

B. M. A. Rahman (S'80–M'82–SM'93), photograph and biography not available at the time of publication.

H. A. El-Mikati, photograph and biography not available at the time of publication.